Numerical simulation of ASR-affected beams: comparison to experimental data

Jean François Seignol, Frédéric Barbier, Stéphane Multon, François Toutlemonde

▶ **To cite this version:**

Jean François Seignol, Frédéric Barbier, Stéphane Multon, François Toutlemonde. Numerical simulation of ASR-affected beams: comparison to experimental data. Proceedings of the 12th International Conference on Alkali-Aggregate Reaction in Concrete, Oct 2004, Beijing, China. pp. 198-206. ⟨hal-03187248⟩

HAL Id: hal-03187248

https://hal.science/hal-03187248v1

Submitted on 31 Mar 2021

HAL is a multi-disciplinary open access archive for the deposit and dissemination of scientific research documents, whether they are published or not. The documents may come from teaching and research institutions in France or abroad, or from public or private research centers.

L'archive ouverte pluridisciplinaire **HAL**, est destinée au dépôt et à la diffusion de documents scientifiques de niveau recherche, publiés ou non, émanant des établissements d'enseignement et de recherche français ou étrangers, des laboratoires publics ou privés.

HAL Authorization

NUMERICAL SIMULATION OF ASR AFFECTED BEAMS COMPARISON TO EXPERIMENTAL DATA

Jean-François Seignol*, Frédéric Barbier, Stéphane Multon, François Toutlemonde
(Laboratoire central des ponts et chaussées, 58 bld Lefèbvre, 75015 Paris, France)

ABSTRACT:

In the domain of concrete structures such as dams or bridges, there is a strong need for numerical models taking into account the mechanical effects of alkali-silica reaction (ASR). Such a model has been developed by Li and Coussy at the Laboratoire central des ponts et chaussées (LCPC, Public Works Research Agency) and is now available in the FEM-software CESAR-LCPC. In parallel, an important experimental research has been recently carried out at LCPC with Électricité de France (EDF, French Power Company) as a partner. It concerns ASR-affected concrete beams submitted to a moisture gradient. The structures are equipped with a large number of monitoring devices, in order to measure the effects of differential swellings.

The aim of this paper is to present the numerical simulation of these ASR-affected beams, in the case of plain concrete structures. The three steps of the calculations are described: moisture diffusion, heat transfer, then development of ASR, leading to swelling and its mechanical effects. Both chemo-elastic and chemo-plastic models are used, and the numerical results are compared to experimental measurements, including effects of possible variations of the calculation parameters.

Namely, considering the final aim of such numerical tools, which is to provide engineers and infrastructures owners with predictive and reliable re-assessment methods, one shall take into account the scattering and uncertainty of the available data (environmental parameters, heterogeneity of the swelling, etc.). Hence, the sensitivity to errors or variations in the input informations has to be evaluated, which is presented in the case of the above-mentioned plain concrete beams.

Key words: Alkali-silica reaction, FEM-simulation, hydro-chemomechanical-coupling, structural effects, model-sensitivity.

1 INTRODUCTION

Considering the numerous researches dealing with modeling of concrete affected by alkali-silica reaction (ASR), one shall notice the divergence between material-oriented models and structure-oriented ones. The first ones represent now a well-known domain [1], whereas calculation methods designed for structure engineers remain few. However, these last ones are strongly needed by affected structures managers. One of these structure oriented numerical models has been developped by Li and Coussy [2], adapted to the frame of the finite element method (FEM) and set up in the software CESAR-LCPC [3].

The validation of such a model needs well-controlled experimental data. During the last years, the Laboratoire central des ponts et chaussées (LCPC, Public Works Research Agency) conducted a large experimental program on structures affected by ASR and submitted to strong moisture gradient [4, 5]. The available data obtained both on cylindrical specimens and on concrete beams can be compared to numerical results. The present paper focuses on the simulation of the plain concrete beam behaviour. The swelling evolution is fitted thanks to several measurements on homogeneous cores, then introduced into CESAR-LCPC in order to compute the beams strains.

Keeping in mind the final goal of this software, which is to help structures managers to evaluate present and future state of affected constructions, one shall note that available environmental data and mechanical properties are not so well known as for a laboratory experiment. Hence the robustness of the modeling method has to be tested too.

In the next section, the available experimental data

*Phone +33 1 40 43 53 40, fax +33 1 40 43 54 99, e-mail seignol@lcpc.fr

are briefly presented. The ASR-model as well as its coupling with mechanical behaviour are described in the third section. Then the numerical simulations of ASR-affected beams are detailed and the results are discussed and compared to experimental measurement. Finally, the sensitivity of the model is studied by having several environment and material variables varied.

2 EXPERIMENTAL DATA

The experimental data used to validate the numerical method are extensively described in [4, 5, 6]. The goal of this research program was to exhibit the strong influence of moisture on ASR-affected structures. In particular the study of concrete submitted to heterogeneous conditions (some parts drying, other parts in contact with water...) is essential to understand the behaviour of bridges and dams in real conditions. The experimental program consisted then in applying a severe moisture gradient to different simply supported beams: two plain-concrete were affected by ASR and compared to a third one, made of "healthy" concrete with similar mechanical properties. Three other beams had been cast to study the effect of reinforcement in the case of ASR-affected concrete: two reactive beams were equipped with ligth and strong reinforcement, respectively, and a non-reactive beam had the same light reinforcement. A picture of this experiment is presented in Fig. 1.

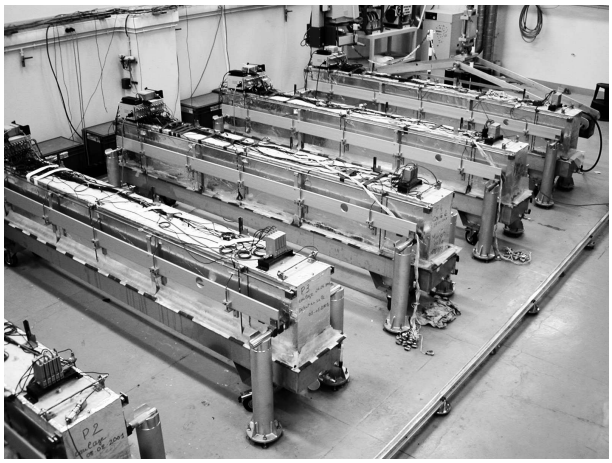

Fig. 1: Beams in controlled atmosphere room.

The several data obtained from beams monitoring are associated with numerous cylindrical and prismatic cores developing free expansion. According to Larive's work [7], concrete swelling depends on available water. Hence, the cores are submitted to three different moisture conditions: complete immersion in water, 100%-RH atmosphere or watertight with aluminium sheets. The ASR-induced expansion is monitored in parallel and perpendicular directions as respects casting direction, to take into account the strong anisotropy of swelling [8]. These cores also provide the classical mechanical parameters of the concrete (Young's modulus, tensile and compressive strength...).

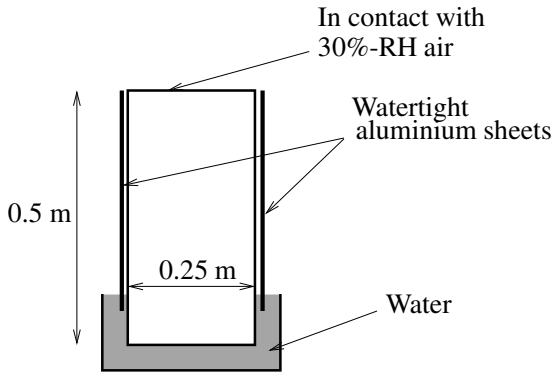

Fig. 2: Cross-section of the beam submitted to moisture gradient.

The simimulations presented in this paper focus on the 3-m long plain reactive concrete beam submitted to a strong moisture gradient. The bottom of the beam is in water, whereas its upper face is in contact with 30% RH (relative humidity) air, as shown on Fig. 2. The lateral faces are sealed. This simple structure has been exposed during 14 months in a constant-temperature room, at 38 ° C in order to generate significant swellings in a short time.

As widely admitted [7], kinetics and intensity of ASR are directly dependent on concrete moisture. Consequently, the lower part of the beam will suffer higher ASR-driven expansion than the upper one, resulting in global bending. Part of this bending is due to differential drying shrinkage; the presence of an unaffected beam similar to the reactive one allows us to tell ASR-induced bending from shrinkage-induced one, taking into account the hypothesis of additive strains.

3 CHEMO-MECHANICAL MODEL

3.1 Modelling ASR-induced expansion

Based on experimental and theoretical studies [7, 9], the re-assessment method to evaluate ASR-affected structures state proposed by Li and Coussy [2] considers that the ASR-degree is characterized by a value $\xi \in [0; 1]$, 0 corresponding to the start of the reaction and 1 representing its end. The ASR-degree leads to imposed expansion ε_χ:

$$\varepsilon_\chi(t) = \beta\xi(t) \tag{1}$$

The evolution of ξ is described by two parameters: τ_l is the latency time of the ASR and τ_c is the characteristic time. The free expansion is then given by Larive's model [10]:

$$\varepsilon_\chi(t) = \beta \frac{1 - e^{-\frac{t}{\tau_c}}}{1 + e^{\frac{\tau_l - t}{\tau_c}}} \tag{2}$$

The values of asymptotic swelling β and timesτ_c and τ_l are strongly related to the thermo-hydric state of the concrete. They are measured for reference temperature T_0 and moisture h_0 on free-swelling sample cores; their values for unspecified temperature T and moisture h can be determined by theoretical and empirical laws [7, 11].

Knowing β, τ_c and τ_l for reference state $(T_0; h_0)$, the first step of an ASR-affected structure calculation consists in determining the RH field $h(t, \mathbf{x})$ and the temperature field $T(t, \mathbf{x})$, where $t \in [0; t_F]$ represents the time and the vector $\mathbf{x}$ corresponds to a location in the concrete structure. Here the determination of these fields is computed for discrete times t_i, $i \in \{0, \ldots, n\}$, $t_0 = 0$, $t_n = t_F$ thanks to the non-linear diffusion modulus of the FEM-software CESAR-LCPC.

Then, these fields are used as input values for a specific modulus in CESAR-LCPC, called ALKA [2]. This modulus computes for each point $\mathbf{x}$ of the structure and for each discrete time t_i the value of ASR-degree ξ and therefore prescribed swelling ε_χ. Last, the mechanical problem is solved taking into account the chemo-mechanical coupling.

3.2 Chemo-mechanical coupling

This imposed swelling is introduced into mechanical models. The ALKA modulus offers two types of constitutive equation for ASR-affected concrete: an elastic one, and a plastic one based on Willam-Warnke yield criterion. These models are described in [2]; their properties are briefly sumarized.

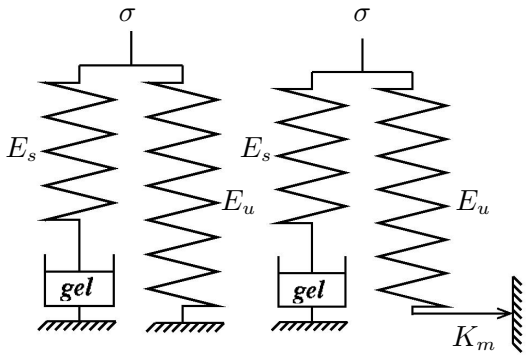

Fig. 3: Chemo-mechanical coupling in unidimensional models

As can be seen on Fig. 3, they assume that the swelling gel creates a pression in a pore whose elastic strain is governed by the Young's modulus E_s. Around it, the solid skeleton resists to the pore expansion and to the externally applied stress σ. This resistance can be elastic, with Young's modulus E_u, or elastoplastic, with Young's modulus E_u and yield strength K_m, in order to represent crack openings caused by internal swelling. Li and Coussy show that these models are equivalent to the following constitutive equations: in the chemo-elastic case,

$$\sigma = E\,(\varepsilon - \varepsilon_\chi) \tag{3}$$

and in the chemo-plastic case,

$$\begin{cases} \sigma + \sigma_\chi = E\,(\varepsilon - \varepsilon_p) \\ \sigma_\chi = E\,\varepsilon_\chi \end{cases} \tag{4}$$

where σ and ε are the material stress and strain, respectively. The parameter E is the concrete Young modulus and ε_p is the irreversible strain, as determined in the classic plasticity theory.

4 NUMERICAL SIMULATIONS

4.1 ASR-induced expansion model

The first step to re-assess an ASR-affected structure consists in determining the free expansion parameters in standard conditions. The experimental program [5] included several specimens in different environmental conditions: in water (denoted by [W] on the following figures), in 100% RH atmosphere ([H]) and sealed under aluminium sheets ([S]). In each case, the temperature was 38 ° C.

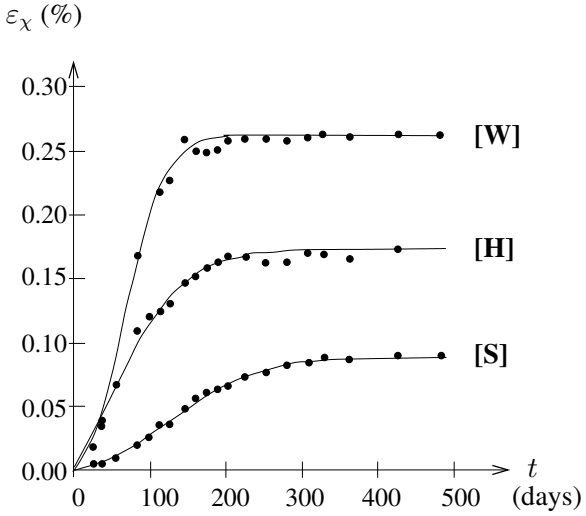

Fig. 4: Free expansion parameters fitting

Specimens were drilled in two directions: perpendicularly to casting direction (horizontal drilling), and parallel to it (vertical). The values of β, τ_c and τ_l of free expansion are determined in each case by least-squares fitting applied to Eq. (2). Results of this identification for the vertical direction are represented in Fig. 4. Let us point out that more precise methods have also been used for this, such as weighted least-squares fitting; the accuracy increase is unsignificant.

The results presented on Table 1 are obtained by average on 3 different cores each, to take into account the scattering of swelling [8].

As explained above, ALKA needs the values of the different parameters for a reference state corresponding to a temperature of 38 ° C and a RH of 100%. In its

present state, the software considers only an isotropic swelling model.

Table 1: Swelling parameters fitted from core samples

direction	environment	β (%)	τ_c (days)	τ_l (days)
vert.	[H]	0.173	49	45
	[W]	0.260	30	67
	[S]	0.116	72	118
horiz.	[H]	0.120	51	47
	[W]	0.137	40	55
	[S]	0.046	47	109

The strong anisotropy of the concrete [1, 8] leads us to use as an average value the resulting volumetric expansion derived from horizontal and vertical results:

$$X_{\text{iso}} = \frac{1}{3}X_{\text{vert}} + \frac{2}{3}X_{\text{horiz}} \tag{5}$$

where X represents any parameter, the subscript *iso*, *vert* and *horiz* refering to isotropic modell, vertical behaviour and horizontal behaviour respectively.

At this point, one shall notice that the material data are more precise than the ones available for real constructions affected by ASR. In these last cases, inverse problem technics are required [12] to fully determine the swelling parameters of the concrete because when the core are drilled from the structure, the initial swelling is unknown. Here, the core expansion has been monitored since its beginning.

4.2 General considerations

The problem to be modelled consists in a 3-m long beam simply supported on both extremities. The temperature field is uniform, and the moisture state depends only on the vertical coordinate. Hence the computations are made on a mesh representing one quarter of the beam, as shown in Fig. 5.

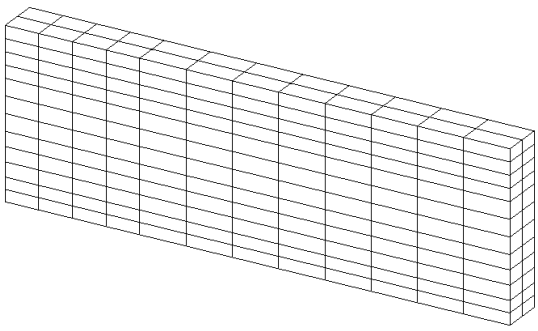

Fig. 5: Mesh representing one quarter of the beam

It is composed of quadratic solid elements organized as follows: 12 elements along the vertical direction Oz in order to model the strong gradients, 12 elements in the longitudinal direction Ox to take into account the structural consequences of differential swelling, and 2 elements in the transversal direction Oy, since this direction does not strongly influence the other ones. This leads to a 1,781 nodes mesh.

After casting, the beam has been kept 28 days curing at 20 °C under totally watertight condtions. It can be assumed that ASR-degree is quite neglectible during that time. Then the beam is installed in controlled-atmosphere room (temperature of the air is $T_a = 38\,^\circ$C and moisture is $h_a = 30\%$), its upper face is unsealed and exposed to the ambiant air, while the lower face is immersed into water. This is considered as initial time $t_0 = 0$. The beam is left during 435 days in these conditions. A middle way between computation time and results accuracy leads to choose a time step of $\Delta t = 15$ days, then each computation is done with $n = 29$ steps.

4.3 Thermal and hydric calculations

At the beginning of the experiment, the beams environment jumps quickly from 20 °C to 38 °C. Experimental observations show that thermal equilibrium is reached in less than 48 hours in the core of the beams. Hence, the thermal problem can be quickly computed with simple asumptions. Considering a linear behaviour of the concrete as respects heat transfer, the temperature field is taken constant and uniform whithin the whole beam.

In opposition, the water diffusion problem is far more complex. This phenomenon is well known to be non-linear [13, 14, 15]. Nonetheless, we start with a simplified approach, since the fitting of complex non linear models might be a long and difficult task. Experimental results [16] exhibit two major processes in the beam.

Initially, the moisture field is uniform, about $h_i = 98\%$. At t_0, the upper face starts to dry. This drying lasts during the whole 435 days and affects an upper layer of approximately 0.14 m. In the same time, the lower part absorbs water by capillarity, resulting in a 100% saturated concrete zone growing up. The kinetics of both phenomena is different. So, in order to confine our computations to linear models, we divide the mesh into two parts, each one with different but constant permeabilities $K_{1,2}$ and moisture capacities $C_{1,2}$ where the subscripts 1 and 2 refer to the upper and lower zones of the beam, respectively. The values of these parameters are chosen thanks to experimental data provided by gammadensimetry and global weighing realized on the beams during the whole experiment [4, 17].

In each part of the beam, the following partial differential equation is solved by the FEM-software CESAR-LCPC:

$$C_{1,2}\frac{\partial h}{\partial t} = \text{div}\,(K_{1,2}\mathbf{grad}h) \tag{6}$$

with the initial condition

$$\forall \mathbf{x}, \quad h(0, \mathbf{x}) = h_i \tag{7}$$

and the boundary conditions:

- $\mathbf{grad}h = \mathbf{0}$ on the lateral faces sealed by aluminium sheets,
- $\mathbf{grad}h = \mathbf{0}$ on the lateral faces corresponding to the longitudinal and mid-span symmetry planes,
- $h = 100\%$ on the lower face, because the presence of liquid water saturates the concrete,
- $h = h_a$ on the upper face, which assumes immediate equilibrium between surrounding atmosphere and air in the pores of the upper concrete layer.

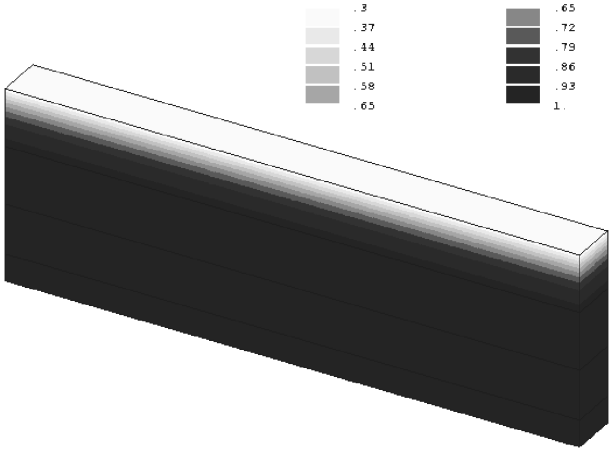

Fig. 6: Relative humidity distribution in the beam after 435 days.

As shown in Fig. 6, the numerical simulation results in a strong drying gradient located in the 15 cm-thick upper-layer of the beam. Nonetheless, the above-mentionned asumption of piecewise-linear behaviour turns out to be insufficient to fit both this drying gradient and the global weight variation of the beam.

4.4 Chemo-elastic simulation

The beams are only loaded by their own weight which leads to very low stresses (less than 0.3 MPa). Considering the 2.8 m span relatively to the cross-section dimensions (0.25 m wide, 0.50 m high), their behaviour is clearly in the elastic domain at the beginning of the experiment. One shall assume that a chemo-elastic behaviour is a fairly good asumption.

The swelling parameters are taken from Table 1 with isotropic values as described by Eq. (5) :

$$\beta = 0.135\%, \quad \tau_c = 50\,\text{days}, \quad \tau_l = 46\,\text{days}$$

The mechanical parameters used in constitutive equation (3) are Young's modulus E and Poisson's ratio ν. A problem could arise with the first one since ASR development results in significant material stiffness loss [10]. In this case, an important decrease of E has been observed [5], from 37.3 GPa at the beginning of the experiment to 29.7 GPa one year later. Fortunately, in this case, the beam is simply supported, which implies that its deformation does not depend on its Young's modulus, as it has been shown both by analytical simplified calculations [5] and by FEM-simulation. The following computations are all made with initial Young modulus and Poisson's ratio:

$$E = 37.3\,\text{GPa}, \quad \nu = 0.22$$

The boundary conditions are:

- vertical displacement equal to 0 at the node corresponding to the simple support,
- normal displacements equal to 0 on the two planes of symmetry,
- null stress on the other faces.

In order to compare numerical results to experimental data, we only compute ASR-induced strains. In fact, the total strain is the sum of ASR-induced ones, of drying shrinkage, of thermal dilatations and of instantaneous effects of self-weight. The reference state of the monitoring devices is chosen once the beam is installed on its supports and in thermal equilibrium with the atmosphere, so the last two terms of the strain are not measured thence they must not be taken into account in the computation. The drying shrinkage is measured on a non-reactive beam placed in identical conditions. The ASR-induced strains can then be obtained by substraction and compared to numerical results.

The effect of differential ASR resulting from moisture gradient after 435 days can be seen in Fig.7.

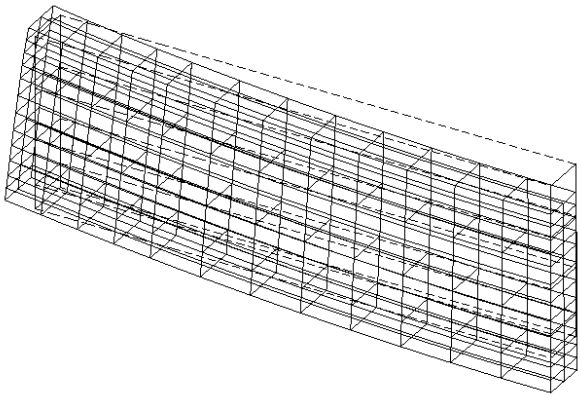

Fig. 7: Beam deformation caused by differential ASR. The maximum deflection is equal to 2.3 mm.

In order to compare numerical results to experimental observations, three characteristic variables are chosen:

- deflection at mid-span δ, equal to the vertical displacement of the node at the middle of the lower part of the mid-span cross-section,
- mean longitudinal strain ε_L, equal to the longitudinal displacement u_x of the point corresponding to the simple support divided by its distance to the mid-span symmetry plane,
- vertical strain at mid-span ε_V, equal to the difference of the vertical displacements u_z of two points in the mid-span cross-section, one on the top of the beam, one on its bottom.

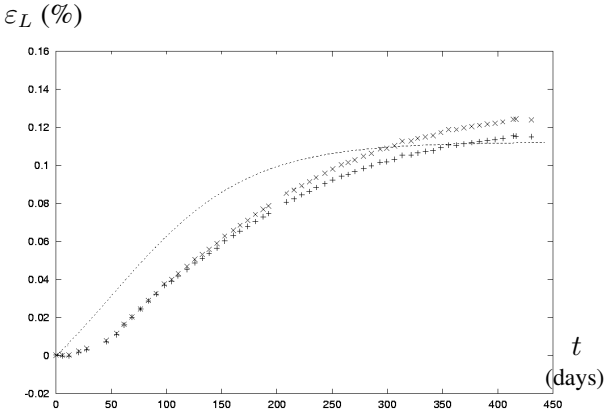

Fig. 8: Elastic model: longitudinal strain versus time. Crosses represent experimental values, dashed line the numerical result.

As can be seen in Fig. 8, the numerical simulation gives fairly good results as concerns strains amplitude, whereas the kinetics of global expansion seems slightly overestimated. The experimental data are represented by two series of crosses: during the experiment, these strains are monitored by two stiffness-free vibrating-wire sensors [4], one on each side of the beams, resulting in slightly different values. It illustrates the numerical discrepancy compared to the experimental uncertainity.

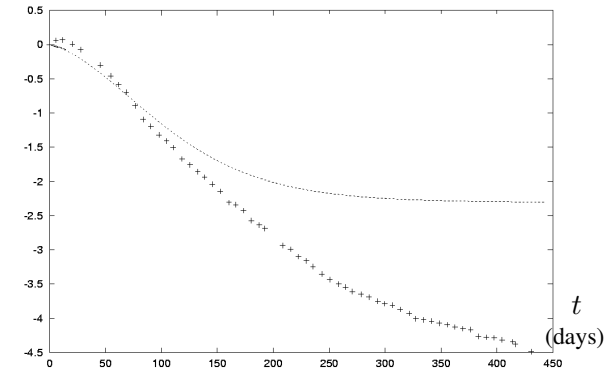

Fig. 9: Elastic model: deflection at mid-span versus time. Crosses represent experimental values, dashed line the numerical result.

The same type of conclusion may be drawn from Fig. 9 which represents the deflection at mid-span. Once again, the kinetics of the deformation is slightly over-estimated by FEM-computation. Moreover, for $t > 150$ days, the computed deflection is largely under-estimated: it stays under 3 mm whereas beam monitoring shows deflection more than 4.5 mm. This date of 150 days corresponds to the onset of cracks on lower face, caused by tensile stresses exceeding concrete tensile strength. In fact, computations lead to tensile stresses up to 10 MPa in the lower part and 23 MPa near the upper face!

This last result might be caused by the inadequacy of the elastic model.

4.5 Chemo-elastoplastic simulation

In order to take into account the onset of crackings, a simulation using elastoplastic constitutive equation is chosen. A classical yield criterion for concrete is William-Warnke's [18]. Its shape is defined by three points f_c, f_{bc} and f_t corresponding to uniaxial compressive strength, biaxial compressive strength and tensile strength respectively. The values of f_c and f_t are known thanks to laboratory tests [5], while f_{bc} might be approximated by the classical relation

$$f_{bc} \approx 1.2\, f_c \tag{8}$$

In the case of this experiment, the dominant nonlinear phenomenon is the cracking of concrete in tension; compressive stresses caused by ASR-induced swelling remain far under their limit value f_c. Hence there is no use in modelling concrete strain softening observed in compression, while the tensile softening plays an important role in material behaviour. We use the exponential softening proposed in [18] where the softening variable z, connected to the volumetric plastic strain, obeys to the following rule:

$$z = z_0 + (z_u - z_0)\left(1 - e^{-k\mathrm{tr}\varepsilon_p}\right) \tag{9}$$

The following computations are made with these parameters:

$$f_c = 38.4\,\mathrm{MPa} \quad f_t = 3.2\,\mathrm{MPa} \quad f_{bc} = 46.6\,\mathrm{MPa}$$
$$z_0 = 1 \qquad z_u = 0.1 \qquad k = 1000$$

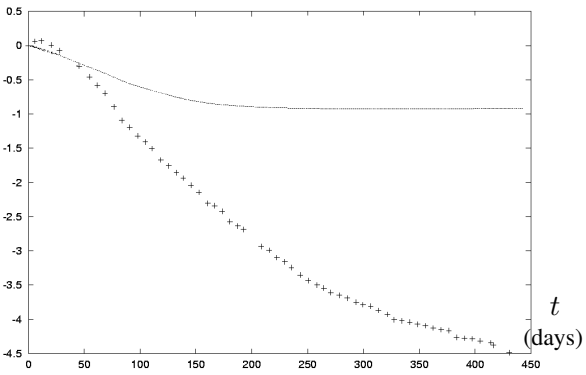

Fig. 10: Elastoplastic model: deflection at mid-span versus time. Crosses represent experimental values, dashed line the numerical result.

Strains computed by this plastic model are comparable to those obtained with the elastic calculation. Naturally, the stresses are more realistic, being kept under the yield point. Unfortunately, as can be seen in Fig. 10, the deflection is more under-estimated than the one computed with the elastic model.

This unsatisfactory result leads us to consider that the main responsible for the previous divergence between computations and experiments is not the constitutive model but the determination of the moisture field. The swelling law presented in Eq. (2) and its parameters seem to be adequate, since global swelling of the beam is correctly simulated, as shown in Fig. 8 (and similar results with ε_V or with the plastic model, as represented in Fig. 11). But the deflection at mid-span is induced by the difference of swelling in upper and lower part of the beam, directly connected to moisture gradient in the beam.

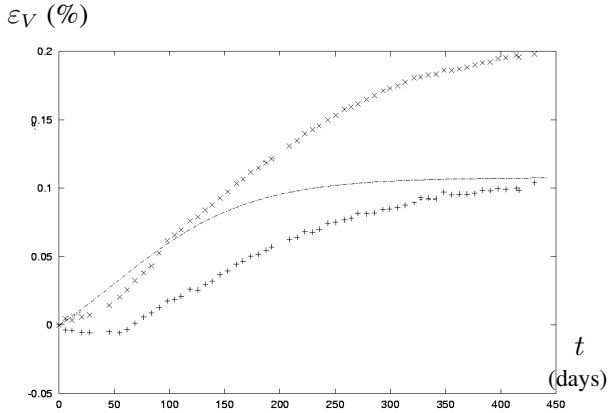

Fig. 11: Elastoplastic model: vertical strain versus time. Crosses represent experimental values, dashed line the numerical result.

It shall be reminded here that the moisture transfer model we used is piecewise-linear, which seems to be too optimistic *a posteriori*. Considering now an under-estimated moisture gradient, it is then possible to explain the large difference of deflections between elastic and plastic computation. Neglecting details, a rough idea of the deflection cause is

1. ASR-induced swelling in the lower part,
2. absence of longitudinal strains in the upper part because of the drying.

But when the lower part expands, it tries to stretch the upper part too, which results in tensile stresses. In the elastic case, these tensile stresses are unbounded, reaching unrealistic values as large as 23 MPa. In the plastic computation, these stresses are limited to f_t. Once this yield point is reached, the swelling lower part can induce strains in the upper part without any further resistance of the plastified and softening concrete. Basically, the lower part of the beam is equally stretched in both cases, but the upper one is more stretched in the plastic computation, resulting in lower deflection.

The divergence between numerical and experimental results could also be explained by other asumptions used in the models. The role played by expansion anisotropy and the coupling between stress-state and ASR-effects cannot be neglected, as shown by recent works [6].

5 SENSITIVITY OF THE MODEL

5.1 Variations of the input parameters

The final aim of a software-modulus such as ALKA is to provide structure managers with tools for re-assessment and prediction of ASR-affected constructions. In these cases, contrary to laboratory samples, the knowledge of input parameters of the computation is partial, uncertain, noisy... The question of how these input errors propagate through the re-assessment process described above shall be precisely and quantitatively addressed.

The input parameters might be split into two categories.

- Environmental parameters deal with the computation of temperature and moisture fields, as boundary conditions. They are often difficult to determine precisely, as most of the structures are not equipped with adequate sensors.
- Material parameters, which concern the three problems: hydrics, thermal and mechanics. They can be easier to obtain, thanks to core samples drilled out of the structure, but one shall keep in mind the heterogeneity of the material, especially with respect to swelling parameters β, τ_c and τ_l [8].

In order to quantify the variations of the output values versus the input, four results are studied: the three previous values, which are deflection at mid-span δ, mean longitudinal strain ε_L and vertical strain in mid-span cross-section ε_V, as well as the maximum compressive stress in the cross-section σ_c. Each of these variables is taken for $t = 435$ days, which corresponds to the last time-step. In the next subsections, the sensitivity study is reported in the following way: let λ be one of the input parameters, with value λ_0 in the reference computation (the chemo-elastic modelling presented in subsection 4.4 with the hydraulic computation as described in subsection 4.3). Let also μ be one of the four above-mentioned outputs, which is equal to μ_0 with the reference computation. The variations of μ/μ_0 versus λ/λ_0 are presented.

5.2 Sensitivity to environmental parameters

In the present case, the environmental parameters reduce to moisture conditions. The temperature is uniform and constant in the whole structure, so a misestimation of its value is equivalent to a variation of the material parameters τ_c and τ_l.

Two input parameters have been varied concerning the hydric problem, the air moisture h_a, whose reference value is $h_{a0} = 0.3$, and the initial moisture of the concrete beam h_i with reference value $h_{i0} = 0.98$. By having h_a varied between $0.33\,h_{a0}$ and $1.33\,h_{a0}$ and h_i between $0.61\,h_{i0}$ and $1.02\,h_{i0}$, the strong sensitivity of the computation to the moisture boundary conditions can be emphasized, as illustrated on Fig. 12.

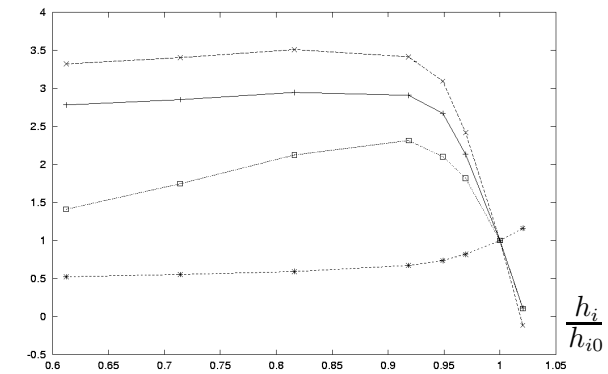

Fig. 12: Relative variations of output parameters versus initial concrete moisture ($+$ is δ, $\star$ is ε_L, $\times$ is ε_L and $\square$ represents σ_c).

Concerning this figure and the next one, only points correspond to real computations. Lines between them are just here for the sake of clearness and are not significant.

5.3 Sensitivity to material parameters

The material parameters are the hydric permeability K, the characteristics β, τ_c and τ_l and the mechanical properties E and ν. Elastic parameters have no direct influence in the present case. Moreover, determining the Young modulus is not the most difficult point in a structure re-assessment. Following variations of the input parameters have been carried out:

- permeability K: from $0.33\,K_0$ to $3.\,K_0$,
- asymptotic swelling β: from $0.07\,\beta_0$ to $2.90\,\beta_0$,
- characteristic time τ_c: from $0.40\,\tau_{c0}$ to $2.00\,\tau_{c0}$,
- latency time τ_l: from $0.42\,\tau_{l0}$ to $2.12\,\tau_{l0}$.

The sensitivity to the material parameter is smaller and more regular than to the moisture conditions: in each case, the output varies like the input,

$$\frac{\mu}{\mu_0} \approx \frac{\lambda}{\lambda_0} \tag{10}$$

or does not vary (for instance, a change in τ_l or τ_c has no influence on ε_L). This behaviour is well represented by the influence of β, as shown on Fig. 13.

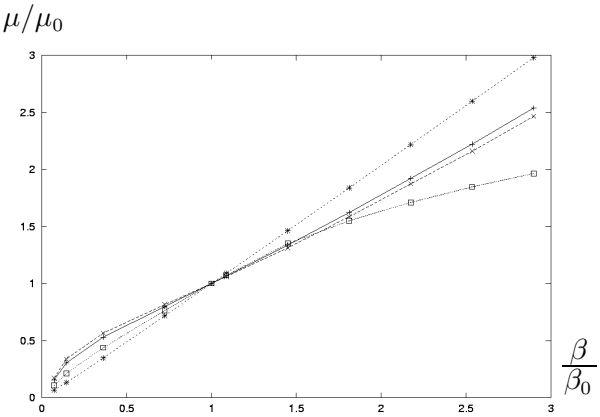

Fig. 13: Relative variations of output parameters versus asymptotic free expansion ($+$ is δ, $\star$ is ε_L, $\times$ is ε_L and $\square$ represents σ_c).

6 CONCLUSIONS AND RECOMMANDATIONS

This paper presents the numerical modeling of ASR-affected concrete structures. It is based on the FEM-software CESAR-LCPC and especially the specific modulus ALKA and its links with heat and hydric transfer problems (DTNL modulus). It has been focused on three points:

- The computations were first aimed to model a fully-monitored experiment on simple structures affected by ASR [5] and to compare their results to the experimental data, for sake of validation.
- The different steps of the computation (thermo-hydric transfers, swelling parameters determination, chemo-mechanics coupling) and the links between them have been explained and considered in the frame of the method proposed by Li and Coussy [2].
- In order to take into account the unavoidable uncertainty of parameters determination in the case of real structures, the global sensitivity of the method has been evaluated and quantified.

The numerical results seem fairly satisfactory in terms of global strains as well as of structural consequences such as beam deflection. Both kinetics and amplitude of the phenomena are correctly approximated by the computation. Despite, some significant divergences occured between numerical simulation and experimental data. A first analysis tends to put the blame on the difficult modeling of the moisture field in the structure. This assumption will deserve deeper investigations.

The sensitivity analysis corroborates this last remark: while the method is dependent on the material parameters according quasi-linear laws, it exhibits in the situation considered an erratic behaviour as the moisture conditions vary.

Over this central question of moisture influence, several improvements for the ALKA modulus shall be outlined: explicit consideration of drying shrinkage, swelling anisotropy, coupling between stress and ASR-effects, etc.

Finally, these works lead to put the stress on the very important role played by water movements in the ASR-affected concrete. Their critical influence and their connections with swelling development have been also emphasised by other recent works [19]. Hence strong recommandations shall be addressed to the structure managers concerning this point. A good moisture monitoring of structures and a precise evaluation of moisture fields used as chemo-mechanics input data is deeply needed to perform a correct ASR-affected structure re-assessment.

REFERENCES

[1] Michelle Moranville-Regourd. Modelling of expansion induced by ASR – new approaches. *Cement and Concrete Composites*, 19:415–425, 1997.

[2] Kefei Li and Olivier Coussy. Concrete ASR degradation: from material modelling to structure assessment. *Concrete Science and Engineering*, 4:35–46, 2002.

[3] Pierre Humbert. Un code général de calcul par éléments finis. *Bulletin de liaison des laboratoires des ponts et chaussées*, 160:112–116, 1989.

[4] Catherine Larive, François Toutlemonde, Michel Joly, André Laplaud, François Derkx, Éric Merliot, Stéphane Multon, Éric Bourdarot, Stéphanie Prené, and Alain Jeanpierre. Structural effects of ASR in France on real and laboratory structures. In *11th Int. Conf. on Alkali-Aggregate Reaction*, pages 979–988, Quebec, 2000.

[5] Stéphane Multon, Jean-François Seignol, and François Toutlemonde. Large girders subjected to alkali-silica reaction. In V. M. Malhotra, editor, *6th Canmet – Int. Conf. on Durability of Concrete*, pages 299–318, Thessaloniki, June 2003. ACI.

[6] Stéphane Multon. *Évaluation expérimentale et théorique des effets mécaniques de l'alcali-réaction sur des structures modèles*. PhD thesis, Université de Marne-la-Vallée, 2003.

[7] Catherine Larive, André Laplaud, and Olivier Coussy. The role of water in alkali-silica reaction. In *11th Int. Conf. on Alkali-Aggregate Reaction*, pages 61–69, Quebec, 2000.

[8] Catherine Larive, Michel Joly, and Olivier Coussy. Heterogeneity and anisotropy in ASR-affected concrete; consequences for structural assessment. In *11th Int. Conf. on Alkali-Aggregate Reaction*, pages 969–978, Quebec, 2000.

[9] Franz-Josef Ulm, Olivier Coussy, Kefei Li, and Catherine Larive. Thermo-chemo-mechanics of ASR expansion in concrete structures. *J. Eng. Mech.*, 126(3):233–242, 2000.

[10] Catherine Larive. *Apports combinés de l'expérimentation et la modélisation à la compréhension de l'alcali-réaction et de ses effets mécaniques*. Number OA28 in Études et recherches. Laboratoire central des ponts et chaussées, Paris, 1998.

[11] Kefei Li, Franz-Josef Ulm, Olivier Coussy, Catherine Larive, and Lichu Fan. Chemoelastic modelling of alkali-silica reaction in concrete. In *11th Int. Conf. on Alkali-Aggregate Reaction*, pages 989–998, Quebec, 2000.

[12] Kefei Li and Olivier Coussy. Numerical assessment of ASR-affected durability of concrete structures. In H.A. Mang, F.G. Rammerstorfer, and J. Eberhardsteiner, editors, *Proc. of the 5th World Congress on Computational Mech.*, Vienna, 2002.

[13] Z. P. Bažant and L. J. Najjar. Nonlinear water diffusion in nonsaturated concrete. *Materials and Structures*, 5(25):3–20, 1972.

[14] R. Mensi, P. Acker, and A. Attolou. Séchage du béton : analyse et modélisation. *Materials and Structures*, 21:3–12, 1988.

[15] V. Baroghel-Bouny, M. Mainguy, T. Lassabatere, and O. Coussy. Characterization and identification of equilibrium and transfer moisture properties for ordinary and high-performance cemetitious materials. *Cement and Concrete Research*, 29:1225–1238, 1999.

[16] Stéphane Multon, Jean-François Seignol, and François Toutlemonde. Concrete girders under severe drying. In *Proc. 4th Int. Conf. on Concrete under Severe Conditions (to be published)*, Seoul, Korea, 2004.

[17] Stéphane Multon and François Toutlemonde. Water distribution in concrete beams. *Material and Structures*, (to be published), 2003.

[18] Franz Josef Ulm. *Un modèle d'endomagement plastique : applications aux bétons de structure*. Number OA19 in Études et recherches. Laboratoire central des ponts et chaussées, 1996.

[19] Stéphane Poyet. *Étude des ouvrages en béton atteints par la réaction alcali-silice - Approche expérimentale et modélisation multi-échelles des dégradations dans un environnement hydro-chemo-mécanique variable*. PhD thesis, Université de Marne-la-Vallée, 2003.